


Nanomolding of Crystalline Metals: The Smaller the EasierZe Liu,^{1,2,*} Guoxing Han,¹ Sungwoo Sohn,³ Naijia Liu,³ and Jan Schroers^{3,†}¹*Department of Engineering Mechanics, School of Civil Engineering, Wuhan University, Wuhan, Hubei 430072, China*²*State Key Laboratory of Water Resources and Hydropower Engineering Science, Wuhan University, Wuhan 430072, China*³*Department of Mechanical Engineering and Materials Science, Yale University, New Haven, Connecticut 06511, USA* (Received 8 July 2018; published 22 January 2019)

We report on a thermomechanical nanomolding method for crystalline metals. Quantified by the aspect ratio, this process becomes easier with decreasing mold diameter. As the responsible underlying diffusion mechanism is present in all metals and alloys, the discovered nanomolding process provides a toolbox to shape essentially any metal and alloy into a nanofeature. Technologically, this highly versatile and practical thermomechanical nanomolding technique offers a method to fabricate high-surface-area metallic nanostructures which are impactful in diverse fields of applications including catalysts, sensors, photovoltaics, microelectronics, and plasmonics.

DOI: [10.1103/PhysRevLett.122.036101](https://doi.org/10.1103/PhysRevLett.122.036101)

Molding is a manufacturing process in which a pliable or moldable material is formed to replicate a mold. It is used as a processing technique for all major material classes, and as the most versatile manufacturing technique for the shaping of thermoplastics. The moldability of a material is typically associated with its flowability. Such flowability is high in thermoplastics, gels, and some glasses; however, it is low in crystalline metals [1,2]. Metals are either too hard in their crystalline state or too fluid and reactive in their liquid state to be considered for molding. The difficulty of a shape to be molded can be quantified in the aspect ratio between the mold cavity depth, L , and the mold cavity diameter, d . In general, molding is increasingly challenging with decreasing d , which can originate from capillary forces [3] or intrinsic size effects, typically related to the length scale of flow units [4]. Such flow units can be grains in crystalline metals (typically microns) or chain length in plastics (typically nanometers), or shear transformation zones in metallic glasses (typically ~ 1 nm). Therefore, attempts to mold on the nanoscale have been limited to thermoplastics [2,5–8], gels [9–11], and glasses [12–15] due to their high moldability and small flow units. Crystalline metals were not considered until recently, where we reported the first evidence that, at a high temperature of $\sim 0.6T_m$, some crystalline metals can be shaped into nanorods [16]. Here, we uncover the underlying mechanism for thermomechanical nanomolding with crystalline metals (TMNM with CMs) as a diffusion dominated mechanism driven by the vacancy concentration gradient which follows the pressure gradient. Diffusion can occur either through a bulk or a surface-interface process, and the ratio of the effectiveness of the two processes depends on the mold diameter and the mold-metal combinations. The scaling of the two processes ($L/d \propto 1/d$ for bulk and $L/d \propto 1/d^{3/2}$ for surface) suggests that molding becomes

easier with decreasing mold size, and that essentially any metal can be molded into high-aspect-ratio and single crystal nanorods, as we show and explain, through TMNM with CMs.

Introduced nanomolding with crystalline metals is a thermomechanical process [Fig. 1(a)], where a piece of crystalline metal is formed against a hard mold under a pressure (typically $p \geq 100$ MPa) and temperature (typically $T \geq 0.5T_m$). By using this method, crystalline metals can be molded into millimeter, micrometer, and nanometer sized features [Fig. 1(b)]. For identical molding conditions, the ease of molding, quantified by the aspect ratio (L/d) of the molded rods increases rapidly with decreasing mold cavity [Figs. 1(b) and 1(c); similar results are shown in Fig. S1 of the Supplemental Material [17] for TMNM with Fe]. This suggests that TMNM with CMs becomes easier with decreasing mold cavity. This is in opposition to other nanomolding methods such as thermoplastic molding of metallic glasses [3,4,18,19], laser shock imprinting [20], liquid printing [21], and dip-pen nanolithography [22], for which smaller and higher aspect-ratio features are typically increasingly challenging.

In general, the dominated deformation mechanism for crystalline metals can be either dislocation slip [23,24], twinning [25,26], or grain boundary sliding or rotation [27,28], depending on the grain size [29]. In our experiments, very few twins are present in the prepared metallic nanorods, and the mold dimension is large compare to the grain size [16]. Therefore, we can rule out twinning, grain boundary sliding or rotation dominated deformation mechanisms. On the other hand, dislocation nucleation and movement will become increasingly less effective with decreasing mold size since the dislocation nucleation rate decreases sharply with decreasing mold diameter [30,31]. Hence, the observed “the smaller the easier” quality of

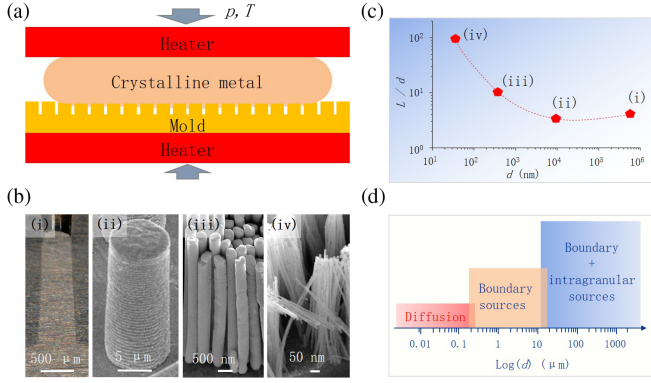


FIG. 1. Scaling of thermomechanical molding with crystalline metals. (a) Schematics of the experimental setup of TMNM with CMs. (b) Thermomechanical molding, taking Ag as an example, with millimeter, micrometer, and nanometer size molds, using molding pressure, temperature, and time of 100 MPa, 620 °C, and 100 s, respectively. Examples of prepared Ag rods with diameters of 0.57 mm, 10 μm , 375 nm, and 36 nm are shown in (i)–(iv). (c) Aspect ratio of the molded Ag rods as the function of mold diameter (d) (the dashed-red line is given as a guide for the eye). (d) The various dominant deformation mechanisms at play during thermomechanical molding at various length scales. Plastic deformation of metals is generally associated with dislocations from grain boundary sources and intragranular sources such as grain sliding and rotating. These processes become decreasingly and rapidly less effective with decreasing mold size. Hence, diffusion becomes the dominant deformation mechanism on the nanoscale.

TMNM with CMs must originate from another mechanism. We suggest, and then quantify, that a mechanism based on diffusion is the underlying mechanism [Fig. 1(d)].

Typically during nanomolding of thermoplastics, gels, and glasses, a decrease of the mold cavity results in additional resistance to materials' flow [3,4]. This has been widely studied for nanomolding with bulk metallic glasses (BMGs) [3,19,32]. Results for a sample system, $\text{Pt}_{57.5}\text{Cu}_{14.7}\text{Ni}_{5.3}\text{P}_{22.5}$, are shown as black solid squares in Fig. 2(a) [4]. The scaling of the moldability, L/d , with the mold diameter for this example is qualitatively different from TMNM with CMs [Fig. 1(c) and red solid pentagons in Fig. 2(a)]. Nanomolding of bulk metallic glasses is based on viscous flow, referred to as Hagen-Poiseuille flow [3,19]:

$$\dot{u}_v \triangleq \frac{dL}{dt} = \frac{1}{64\eta\lambda}(4\gamma \cos\theta + pd) \propto d, \quad (1)$$

where η is the viscosity, $\lambda = L/d$, γ is the surface energy of the supercooled liquid, and θ is the contact angle between the supercooled liquid metals and mold [3,33].

Integrating Eq. (1) with respect to time enables us to quantify $L/d(d)$. Results for nanomolding with BMGs and for TMNM with Au (see the Supplemental Material [17]) are displayed in Fig. 2(a). Obviously, nanomolding with

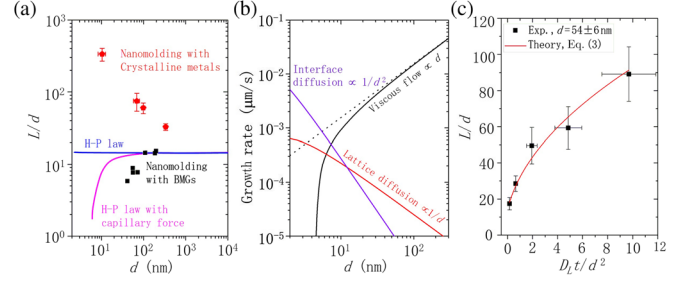


FIG. 2. Deformation mechanism of TMNM with CMs compared to other nanomolding mechanisms. (a) Moldability, quantified by L/d , scales qualitatively differently for bulk metallic glasses (black solid squares; the data are from Ref. [4]), and for crystalline metals (red solid pentagons; the dashed-red line is a guide for the eye). The processing of Au nanorods was carried out at 622 °C under ~ 800 MPa for 100 s. The Hagen-Poiseuille law (H-P law) with capillary force where $\gamma = 1$ N/m and $\theta = 120^\circ$ [10] (magenta line) and without capillary force (blue line) are calculated. The molding time and loading pressure are 180 s and ~ 350 MPa, respectively, taken from Ref. [4]. The discrepancy between theory (magenta line) and experiments (black solid squares) is attributed to an enhanced viscosity on the nanoscale [4]. (b) Calculated growth rates for the diffusion driven growth of Au nanorods at 500 °C [Eq. (2), red and purple lines]. Viscous flow based mechanisms with and without the capillary effect for nanomolding of Pt-BMG are also plotted for comparison [Eq. (1), black and dashed-black lines). The loading pressure and aspect ratio are 500 MPa and $\lambda = 5$, respectively. The other parameters are taken from the literature and are listed in Table S1 of the Supplemental Material [17]. (c) Growth of Au nanorods at 500 °C and ~ 500 MPa versus molding time. The dots represent the experimental data and the solid line is fitted according to Eq. (3).

BMGs is qualitatively different from TMNM with CMs. Nanomolding with BMGs becomes more difficult with a decrease of the mold diameter (or independent without capillary forces ($\theta = 90^\circ$) [4,34]). In sharp contrast, TMNM with CMs becomes easier with decreasing mold size. These quantitatively different behaviors suggest a mechanism for the TMNM with CMs that scales with $1/d^n$ (with $n > 0$). Size comparisons rule out grain boundary sliding or rotation mechanisms [28]. The grain size of the used metals here is on the order of $10^1 \mu\text{m}$ [16], which is at least 2 orders of magnitude larger than the considered mold cavity diameters. Further, the scaling of $L/d(d)$ also excludes dislocation dominated deformation as the underlying dominant mechanism for TMNM with CMs because dislocation nucleation rate and movement rapidly decrease with decreasing d due to the size effect in plasticity [35,36]. A mechanism that scales as $1/d^n$ (with $n > 0$) is diffusion. Taking one-dimensional (1D) random diffusion, e.g., the diffusion distance can be estimated by $L_D = \sqrt{D_b t}$. Substituting typical values for self-diffusivity of Au at 500 °C, of $D_b = 15.7 \text{ nm}^2/\text{s}$ [37], for a typical experimental timescale of 100 s results in a random diffusion length of $L_D \approx 40$ nm. Such an estimation suggests smaller length

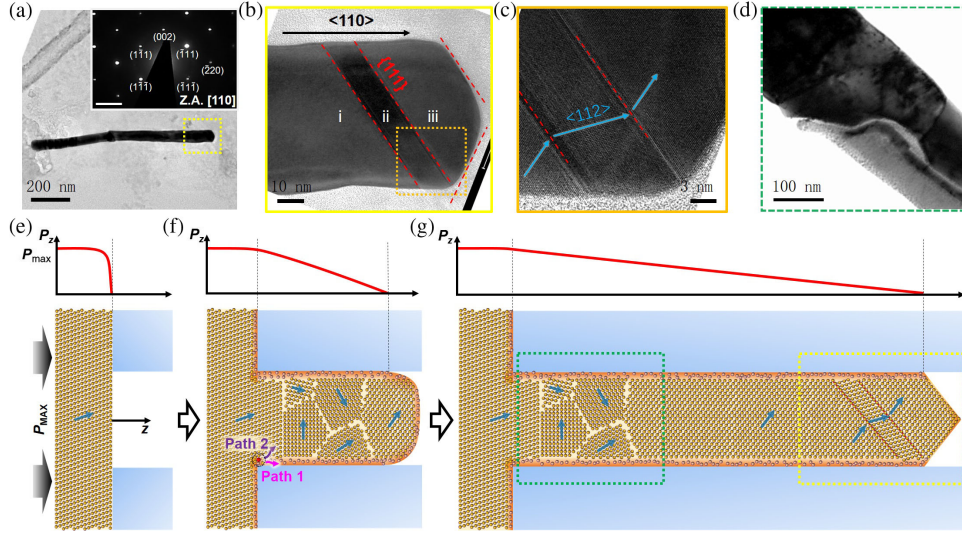


FIG. 3. Atomic growth mechanism of thermomechanical nanomolding with crystalline metals. (a)–(c). TEM images from a diameter of 50 nm Au nanorod fabricated by TMNM. (a) A bright field image of an Au nanorod. (Inset) Its corresponding selected area electron diffraction pattern reveals the growth direction as [110]. The scale bar is $0.41/\text{\AA}$. (b),(c) Enlarged images of the tip region [(b) and (c) are captured from yellow and orange rectangles in (a) and (b), respectively]. Twins are revealed with twin planes of $\{111\}$ close to the tip, and $\{111\}$ facets at the tip. $\{111\}$ planes are marked by red-dashed lines in (b) and (c). $\langle 112 \rangle$ directions are indicated as blue arrows in (c) to highlight mirrorlike symmetrical characteristics on the twin boundaries. Twins can be generated to release local energy or misfit upon growing, which is commonly observed in face-centered-cubic Au. (d) A TEM image from a ~ 100 nm Au nanorod showing multiple grains with different crystallographic orientations at the root of the nanorod. (e)–(g) Schematics of TMNM with CMs indicating atomistic processes as a sequence of growth of a metal nanorod and corresponding pressure profiles along its axis. Blue arrows represent $\langle 112 \rangle$ direction vectors. (e) A feedstock metal (here for fcc) is positioned on the mold at the molding temperature, and a molding pressure is applied. (f) The applied pressure and temperature result in diffusion down the pressure gradient, which causes a vacancy gradient. As the initial orientation of the feedstock metal consists of multiple and randomly oriented grains, growth originally starts along a nonpreferred orientation. This causes nucleation of new grains which progress toward a more preferred orientation (for fcc closer to [110]). There are two possible and size dependent diffusion mechanisms: (i) interface diffusion along the mold-metal interface (path 1) and (ii) lattice diffusion through the rod (path 2). (g) A rod at a later stage of molding which contains small crystals on the root, a long region of a perfect single crystal which can exceed $L/d > 100$, and twins and faceted edges at the tip.

scales than experimentally observed without an overall driving force for diffusion. However, as the pressure varies along the forming nanorod (see Fig. 3), so does the vacancy concentration. Hence, diffusion into the mold cavity is not a random diffusion process but is driven by a gradient of vacancy concentration. Considering that the diffusion of an atom can go through either the lattice or the mold-CM interface [38,39], we separately calculate the growth rates for lattice diffusion and interface diffusion by assuming that vacancy concentration varies only along the axis of the nanorod (1D model; see the Supplemental Material [17]):

$$\begin{aligned} \dot{u}_L &= \frac{p\Omega D_L}{kT\lambda} \left(1 - \frac{2\delta}{d}\right)^2 \frac{1}{d} \propto \frac{1}{d} \text{ for } \delta \ll d; \\ \dot{u}_I &= \frac{4\dot{Q}_I}{\pi d^2} = \frac{4p\Omega\delta D_I}{kT\lambda} \left(1 - \frac{2\delta}{d}\right) \frac{1}{d^2} \propto \frac{1}{d^2} \text{ for } \delta \ll d, \end{aligned} \quad (2)$$

where $\Omega = 4\pi r_0^3/3$ is the atomic volume, r_0 the atomic radius, δ the interface thickness, D_L the lattice diffusion coefficient, and D_I the interface diffusion coefficient.

Equation (2) reveals that both diffusion based mechanisms result in a growth rate inversely proportional to d . Such behavior is qualitatively consistent with our experimental observations (Figs. 1(c) and 2(a), and Fig. S1 of the Supplemental Material [17]). To compare diffusion based growth (lattice and interface) of metallic nanorods with the viscous flow based nanomolding of BMGs, the growth rates for typical nanomolding of Pt-BMG and diffusion based growth of Au at 500 °C are calculated [Fig. 2(b)]. The diffusion controlled mechanism are qualitatively in agreement with our experimental data, whereas the viscous flow behavior is not. When assuming that the interface diffusivity is 10 times faster than the lattice diffusivity, below $d \sim 10$ nm, interface controlled growth would be the more efficient mechanism. However, as the interface diffusivity is unknown and will be highly sensitive to mold-CM combinations, the crossover of interface diffusion dominated growth at ~ 10 nm has a large uncertainty, as it is only estimated and may vary significantly.

To quantitatively compare the diffusion based mechanism with the experimentally determined aspect ratio of metallic nanorods, we add both diffusion processes, as they

can independently and simultaneously occur and integrate Eq. (2) with respect to time, and we get

$$\frac{L}{d} = \sqrt{\left(\frac{L_0}{d}\right)^2 + \frac{2p\Omega D_L t}{kT d^2} \left(1 + 4\frac{D_I \delta}{D_L d}\right)} \text{ for } \delta \ll d. \quad (3)$$

L_0 is the depth of metal filling into the mold when the loading force reaches its maximum value. Equation (3) predicts $L/d \propto t^{1/2}$. To test this prediction, we experimentally varied the molding time while keeping all other processing conditions constant (see the Supplemental Material [17]). We found a good description of Eq. (3) in the experimental data [Fig. 2(c)]. It is worth mentioning that $[\partial^2(L/d)]/\partial t^2 < 0$, indicating a decreasing growth rate with increasing molding time. Such a decrease in the growth rate originates from a decreasing gradient between the pressure at the tip of the nanorod and the pressure above the mold cavity, $\Delta p \approx p/L$. Most importantly, the predictions of Eq. (3) agreeing well with the experimental data reveal that the mechanism of TMNM with CMs is diffusion dominated. However, it must be noted that the lattice diffusion mechanism predicts a size-independent growth length while an interface diffusion mechanism results in a growth length inversely proportional to the mold size [Eq. (3)]. If we plot the experimental data in Fig. 2(a) (red solid pentagons) as $L(d)$ (Fig. S2 of the Supplemental Material [17]), we find that the growth length of Au nanorods is approximately constant—however, with a superimposed term. Such a term, which is proportional to the mold size, can be attributed to dislocation motion as the slip system become increasingly activated with increasing mold size under a high forming pressure of ~ 800 MPa.

To further identify the mechanism for TMNM with CMs and characterize the orientation of the grown nanorod, we used TEM (see the Supplemental Material [17]) [Figs. 3(a)–3(d)]. We found for the considered Au nanorods that all are essentially single crystals growing along [110]. Often, close to the tip, few twins are observed [Fig. 3(c), HRTEM images at local regions (i)–(iii) are shown in Fig. S3 of the Supplemental Material]. The preferred orientation of the Au nanorods along [110] during experimental growth may originate from the anisotropy of self-diffusion in crystalline metals. As the {110} planes are the loosest packed planes, diffusion occurs most rapidly along [110] (see, e.g., Ref. [40]). At the entry of the mold cavity, some small crystals can be found [Fig. 3(d); see also Fig. S4 of the Supplemental Material [17]].

Based on the TEM investigations [Figs. 3(a)–3(d)] and growth scaling and velocity observations (Fig. 2), we propose the following atomic-scale mechanism for TMNM with CMs [Figs. 3(e)–3(g)]: The pressure gradient from entry to tip along the cavity depth results in a vacancy concentration gradient. Diffusion occurs predominately along this gradient. As the feedstock from which the nanorods are molded comprises crystals with random

orientations, a change in orientation is generally required to form the observed [110] nanorods. This occurs at the entrance to the mold cavity, where often several small crystals with “rotating” orientations toward [110] can be observed [Fig. 3(d) and Fig. S4 of the Supplemental Material [17]]. This suggests that the originally growth of nanorods follows the orientation of the feedstock crystal. As this orientation is generally not [110], a faster growing crystal with an orientation closer to or of [110] may nucleate, and eventually [110] oriented crystal forms and prevails to continue to grow into very high aspect-ratio nanorods. During growth, particularly close to the tip or at the branches, twins can be readily formed to maintain the preferred [110] direction with little energy cost, which indicates that shear mechanism based twinning deformation can also contribute to the growth of Au nanorods. However, the very few observed twins in the prepared metallic nanorods (Fig. 3 or Ref. [16]) indicate that the twinning is not the dominated deformation mechanism in TMNM with CMs.

One of the major findings of our work is that molding becomes easier with decreasing mold size, quantified by a decreasing function L/d with d . This scaling naturally results from the scaling of the underlying diffusion controlled mechanism. For lattice diffusion, Eq. (2) suggests that $L/d \propto 1/d$, whereas for interface diffusion $L/d \propto 1/d^{3/2}$. Our data suggests, particularly for $d > 10$ nm, a predominant lattice diffusion dominated mechanism. However, this may be superimposed by an interface diffusion mechanism, particularly for $d < 10$ nm. The effectiveness of the interface diffusion mechanism strongly depends on the mold material and moldable crystalline metal, and hence it can dominate the transport mechanism. In that case, the additional $1/d^{3/2}$ (to the $1/d$) originates from the increasing surface to volume ratio with decreasing d . Experimentally, fabricating the smallest nanofeatures by TMNM with CMs is limited by available molds. For the smallest mold size of 5 nm considered in our experiments, we found that L/d follows the trend suggested by Eq. (3) [Fig. 2(a)], and the aspect ratios of the molded Au nanowires arrays are as high as ~ 340 [Fig. 2(a)].

Besides the capability of TMNM with CMs to fabricate smallest-in-diameter nanorods, another demonstration of versatility requires study of the range of materials that can be formed by TMNM. In opposition to most practical nanofabrication techniques, TMNM should be possible with essentially all metals and alloys, as the underlying diffusion mechanism is present in all metals and alloys. To demonstrate such versatility, we considered various metals, including metals with different crystal structures and alloys ranging to the extreme case of high entropy alloys. Specifically, we considered gold, nickel (fcc), vanadium (bcc), iron (bcc), $\text{Ag}_{75}\text{Ge}_{25}$, $\text{Ni}_{60}\text{Ti}_{40}$, $\text{Cu}_{34.7}\text{Zn}_{3.0}\text{Sn}_{62.3}$, PdCuNi, and PdCuNiPtRhIr [41] (Figs. 4(a)–4(i); see the Supplemental Material [17] for the casting of alloys).

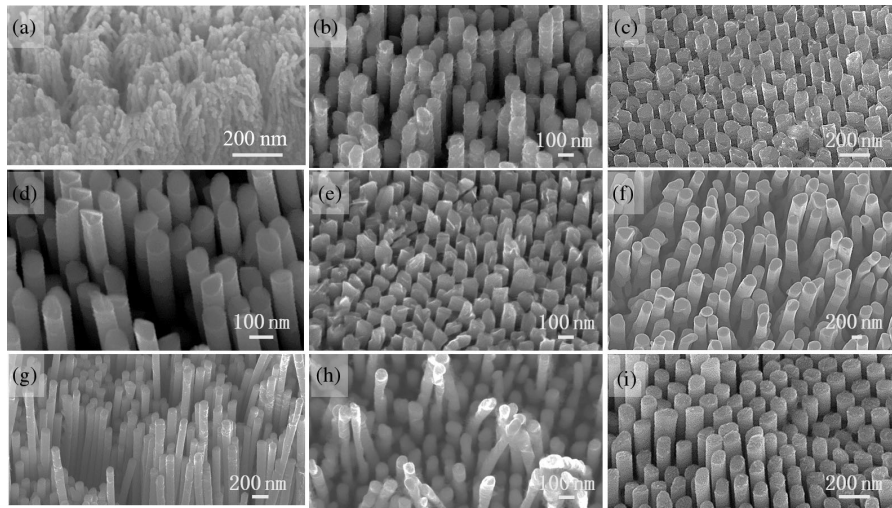


FIG. 4. Examples of fabricated nanorods arrays through TMNM with CMs. (a) Au nanorods of 5–13 nm in diameter, formed under a pressure of ~ 500 MPa at 500°C for 100 s. (b) TMNM with Ni (fcc) at 600 MPa and at 600°C for 240 s. (c) TMNM with V (bcc) at 437 MPa and at 650°C for 100 s. (d) TMNM with Fe (bcc) at 400 MPa and at 600°C for 240 s. (e) TMNM with $\text{Ni}_{60}\text{Ti}_{40}$ at 650°C , under the forming pressure of 800 MPa for 180 s. (f),(g) TMNM with $\text{Ag}_{75}\text{Ge}_{25}$ and $\text{Cu}_{34.7}\text{Zn}_{3.0}\text{Sn}_{62.3}$ at 500°C , loaded to ~ 350 MPa under a constant loading rate of 1.8 mm/min. (h) TMNM with PdCuNi at 695°C , under the forming pressure of 800 MPa for 180 s. (i) TMNM with high entropy alloy (PdCuNiPtRhIr) at 650°C , under the forming pressure of ~ 1000 MPa for 180 s.

For all considered metals and alloys, high-aspect-ratio nanorods can be readily fabricated using TMNM with CMs.

In summary, we revealed the underlying mechanism for thermomechanical nanomolding with crystalline metals as a diffusion controlled growth mechanism. Such a mechanism results in single crystal molding of high-aspect-ratio nanorod arrays and becomes easier with decreasing nanorod diameter. The presence of underlying diffusion mechanism in all metals and alloys suggests that TMNM with CMs is applicable to essentially all metals and alloys. This is different from the vast majority of nanomolding methods, which are typically limited to specific materials and/or by the size and aspect-ratio ranges. Such versatility and practicality of thermomechanical nanomolding with crystalline metals indicate a period of rapid progress and novel exploration of metal based nanomaterials.

Z.L. and G.H. acknowledge the National Natural Science Foundation of China (Grants No. 11602175, No. 11632009, and No. 11872284). Z.L. also acknowledges the support from the “Thousand Youth Talents Plan” in China. S.S., N.L., and J.S. acknowledge the U.S. Department of Energy through the Office of Science, Basic Energy Sciences, Materials Science and Engineering Division (Grant No. DE SC0004889).

*Corresponding author.
ze.liu@whu.edu.cn

†Corresponding author.
jan.schroers@yale.edu

- [1] J. Schroers, T. M. Hodges, G. Kumar, H. Raman, A. J. Barnes, Q. Pham, and T. A. Waniuk, *Mater. Today* **14**, 14 (2011).
- [2] L. J. Guo, *Adv. Mater.* **19**, 495 (2007).
- [3] G. Kumar, H. X. Tang, and J. Schroers, *Nature (London)* **457**, 868 (2009).
- [4] Z. Shao, M. Gopinadhan, G. Kumar, S. Mukherjee, Y. Liu, C. S. O’Hern, J. Schroers, and C. O. Osuji, *Appl. Phys. Lett.* **102**, 221901 (2013).
- [5] P. Ruchhoeft *et al.*, *J. Vac. Sci. Technol. B* **17**, 2965 (1999).
- [6] Y. N. Xia and G. M. Whitesides, *Annu. Rev. Mater. Sci.* **28**, 153 (1998).
- [7] S. Y. Chou, P. R. Krauss, and P. J. Renstrom, *Science* **272**, 85 (1996).
- [8] H. D. Rowland, W. P. King, J. B. Pethica, and G. L. W. Cross, *Science* **322**, 720 (2008).
- [9] M. Diez, P. Mela, V. Seshan, M. Möller, and M. C. Lensen, *Small* **5**, 2756 (2009).
- [10] S. S. Williams, M. J. Hampton, V. Gowrishankar, I. K. Ding, J. L. Templeton, E. T. Samulski, J. M. DeSimone, and M. D. McGehee, *Chem. Mater.* **20**, 5229 (2008).
- [11] O. J. A. Schueller, G. M. Whitesides, J. A. Rogers, M. Meier, and A. Dodabalapur, *Appl. Opt.* **38**, 5799 (1999).
- [12] Y. Saotome and Z. A. I. Tao, *MRS Online Proc. Libr.* **554**, 385 (1998).
- [13] J. Schroers, *Adv. Mater.* **22**, 1566 (2010).
- [14] M. Colburn *et al.*, *Proc. SPIE* **3676**, 379 (1999).
- [15] N. Li, W. Chen, and L. Liu, *JOM* **68**, 1246 (2016).
- [16] Z. Liu, *Nat. Commun.* **8**, 14910 (2017).
- [17] See Supplemental Material at <http://link.aps.org/supplemental/10.1103/PhysRevLett.122.036101> for the details of Eq. (2), TMNM with Au and Fe, TEM characterization, casting of alloys, supplementary Figs. s1–s4, and supplementary Table s1.

- [18] K. Golden, B. Jerzy, and S. Jan, *Nanotechnology* **24**, 105301 (2013).
- [19] Z. Liu and J. Schroers, *Nanotechnology* **26**, 145301 (2015).
- [20] H. Gao, Y. Hu, Y. Xuan, J. Li, Y. Yang, R. V. Martinez, C. Li, J. Luo, M. Qi, and G. J. Cheng, *Science* **346**, 1352 (2014).
- [21] E. Kim, Y. Xia, and G. M. Whitesides, *Nature (London)* **376**, 581 (1995).
- [22] R. D. Piner, J. Zhu, F. Xu, S. Hong, and C. A. Mirkin, *Science* **283**, 661 (1999).
- [23] P. Schall, I. Cohen, D. A. Weitz, and F. Spaepen, *Nature (London)* **440**, 319 (2006).
- [24] V. Yamakov, D. Wolf, M. Salazar, S. R. Phillpot, and H. Gleiter, *Acta Mater.* **49**, 2713 (2001).
- [25] Y. T. Zhu, X. Z. Liao, and X. L. Wu, *Prog. Mater. Sci.* **57**, 1 (2012).
- [26] X. L. Wu, X. Z. Liao, S. G. Srinivasan, F. Zhou, E. J. Lavernia, R. Z. Valiev, and Y. T. Zhu, *Phys. Rev. Lett.* **100**, 095701 (2008).
- [27] Y. Wei, A. F. Bower, and H. Gao, *J. Mech. Phys. Solids* **54**, 2554 (2006).
- [28] T. G. Langdon, *Philos. Mag.* **22**, 689 (1970).
- [29] X. Z. Liao, Y. H. Zhao, Y. T. Zhu, R. Z. Valiev, and D. V. Gunderov, *J. Appl. Phys.* **96**, 636 (2004).
- [30] T. Zhu and J. Li, *Prog. Mater. Sci.* **55**, 710 (2010).
- [31] Q.-J. Li and E. Ma, *Mater. Res. Lett.* **6**, 283 (2018).
- [32] X. Liu, Y. Shao, S. Y. Lu, and K. F. Yao, *J. Polym. Sci. Part B: Polym. Phys.* **53**, 463 (2015).
- [33] S. Ding, J. Kong, and J. Schroers, *J. Appl. Phys.* **110**, 043508 (2011).
- [34] H. M. Chiu, G. Kumar, J. Blawdziewicz, and J. Schroers, *Scr. Mater.* **61**, 28 (2009).
- [35] M. D. Uchic, D. M. Dimiduk, J. N. Florando, and W. D. Nix, *Science* **305**, 986 (2004).
- [36] F. F. Csikor, C. Motz, D. Weygand, M. Zaiser, and S. Zapperi, *Science* **318**, 251 (2007).
- [37] S. M. Makin, A. H. Rowe, and A. D. Leclair, *Proc. Phys. Soc. London Sect. B* **70**, 545 (1957).
- [38] Y. Oishi and W. D. Kingery, *J. Chem. Phys.* **33**, 480 (1960).
- [39] C. Herring, *J. Appl. Phys.* **21**, 437 (1950).
- [40] W. C. Winegard, *Acta Metall.* **1**, 230 (1953).
- [41] S. Sohn, Y. Liu, J. Liu, P. Gong, S. Prades-Rodel, A. Blatter, B. E. Scanley, C. C. Broadbridge, and J. Schroers, *Scripta Materialia* **126**, 29 (2017).